Adsorption (2008) 14: 485–491
DOI 10.1007/s10450-008-9121-1

Liquid-liquid phase separation of binary Lennard-Jones fluid in slit nanopores

Hideki Kanda · Hisao Makino

Received: 15 June 2007 / Revised: 24 March 2008 / Accepted: 28 March 2008 / Published online: 23 April 2008

Abstract The capillary phase separation of a binary mixture of two truncated and shifted Lennard-Jones (LJ) Ar liquids in slit-shaped oxygen nanopores is examined. The LJ parameters—ε(Ar(A)–Ar(A)) = ε(Ar(B)–Ar(B)) = 0.8ε(Ar(A)–Ar(B)) and 0.5ε(Ar(A)–O) = ε(Ar(B)–O)—were used to distinguish the two Ar liquids. The cut off distance for Ar was 3.5σ. We employed a molecular dynamics (MD) technique in which a pore space was connected with a bulk solution to easily determine the equilibrium bulk concentration. Liquid phase isotherms were obtained for pores with widths ranging from 5.5σ to 9.5σ, and the relation between the pore width and the phase separation concentration was determined. Each simulation was run until the bulk concentration attained equilibrium (1–2 μs). The MD results show that the Patrick model overestimates the bulk concentration for a given pore size. We proposed a modified Patrick model in which the pore wall potential is considered. In our model, the Gibbs-Tolman-Koenig-Buff effect is not considered for the interfacial tension since two surfaces of tension exist on both sides of the equimolar dividing surface of the two-Ar liquid phase. The two surfaces of tension neutralized Gibbs-Tolman-Koenig-Buff effect each other. The present simple model successfully describes the relation to prove its reliability.

Keywords Liquid-liquid equilibria · Nanopore · Thermodynamic model · Lennard-Jones · Molecular simulation

H. Kanda (✉) · H. Makino
Energy Engineering Research Laboratory, Central Research Institute of Electric Power Industry, Yokosuka, Kanagawa 240-0196, Japan
e-mail: kanda@criepi.denken.or.jp

1 Introduction

The concept of capillary phase separation (CPS) in pores was proposed by Patrick more than 80 years ago (Patrick and Eberman 1925; Patrick and Jones 1925). This concept had been largely unnoticed until Miyahara et al. experimentally studied it and proposed a similar concept model (Miyahara et al. 1994, 1997a).

They reported that a curved interface should separate two liquid phases in nanopores even for a bulk equilibrium concentration lower than the saturated bulk concentration The potential of interfacial tension balances the bulk potential of the diluted bulk solution. This concept is similar to the modified Kelvin condensation model. For the simplest geometry of the confining space, i.e., a slit pore, their equation is described in the following form:

$$kT \ln \frac{C}{C_s} = -v_B \frac{\gamma}{W/2 - t} \tag{1}$$

Here, k is Boltzmann's constant and T is the temperature. C denotes the concentration in the bulk phase; subscript s, the saturation; γ, the normal interfacial tension of two liquid phases; v_B, the volume per molecule of the adsorbed liquid; W, the pore width; and t, the thickness of the liquid film adsorbed on the pore surface; this equation was introduced by Miyahara et al. (Miyahara et al. 1994, 1997a). In principle, the critical concentration of the CPS must be determined by only the pore size.

However, we consider that the interaction with the pore walls should influence not only the adsorbed liquid film but also the capillary phase, mainly in case of a strongly interactive liquid. In fact, for capillary condensation, the validity of this concept has been confirmed by many studies (Yoshioka et al. 1997; Miyahara et al. 1997b, 2000; Kanda et al. 2000a, 2000b).

The CPS of binary mixtures in porous media have been studied by many simulations (Brochard and De Gennes 1983; Nakanishi and Fisher 1983; De Gennes 1984; Lin et al. 1990; Ma et al. 1992; Keblinski et al. 1993; Zhang and Chakrabarti 1994, 1995; Goada et al. 1995; Strickland et al. 1995; Laradji et al. 1996; Velasco and Toxvaerd 1996; Gelb and Gubbins 1997a, 1997b, 1997c; Sliwinska-Bartkowiak et al. 1997). Valiullin and Furo experimentally studied the NMR (nuclear magnetic resonance) results of CPS in controlled porous glasses and obtained correlations from circumstantial evidence. (Valiullin and Furo 2002) However, none of them have proposed a simple CPS coexistence model.

This study clarifies the following by conducting the molecular dynamics (MD) of Lennard-Jones (LJ) fluids in slit nanopores. Depending on the influence of the attractive potential energy of the pore walls, fluids in slit nanopores showed CPS at a concentration lower than the concentration predicted by Patrick and Miyahara et al. (Patrick and Eberman 1925; Patrick and Jones 1925; Miyahara et al. 1994, 1997a, 1997b).

2 MD simulation in which bulk liquid is realistically in contact with nanopore space

An MD technique suitable for liquid phase isotherm determination in pores is applied in this study. Possible alternatives for molecular simulation would include employing the grand canonical Monte Carlo (GCMC) method, which has often been employed for the determination of adsorption equilibrium. However, the grand potential should be calculated to determine the true thermodynamic equilibrium. Moreover, the interfacial tension between two fluids is a very important factor in CPS. In particular, partially soluble fluids are extremely sensitive to the interface.

Figure 1 shows the unit cell employed in this study. The black part denotes pore atoms; the condensate Ar(B), the strongly interactive liquid with a pore wall; and the bulk liquid Ar(A), the weakly interactive liquid. The unique feature of this cell is that the bulk liquid phase and nanopore space are connected realistically. By using this realistic cell, the formation of the interface becomes inevitable.

Because of this interaction, the equilibrium concentration for a given number of separated molecules can be determined. Further, the simulation cell allows a stable interface to exist. It is possible that because of the presence of the interface in the cell, and the relation between the pore size and the critical concentration for separation could be obtained. We employed a periodic boundary condition in the x and z directions.

Binary truncated and shifted LJ fluids in a slit-shaped pore made of LJ silica were employed as a model system for testing the proposed model. The LJ parameters—$\varepsilon\,(\mathrm{Ar_{AB}}) = 0.8\varepsilon\,(\mathrm{Ar_{AA}}) = 0.8\varepsilon\,(\mathrm{Ar_{BB}})$ and $0.5\,\varepsilon(\mathrm{Ar_A}\text{–}\mathrm{O}) = \varepsilon\,(\mathrm{Ar_B}\text{–}\mathrm{O})$—were used to distinguish between the two Ar liquids. The cut off distance between the two Ar liquids was 3.5σ (Ar) and that between Ar and O was 3.5σ (Ar–O).

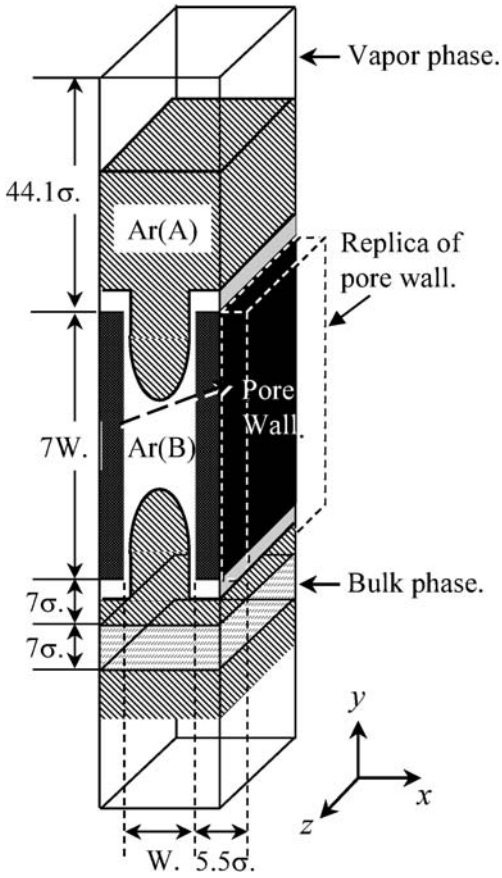

Fig. 1 Schematic figure of unit cell

Interactions with silicon atoms were neglected and only the bound oxygen atoms were considered as the interaction sites, as assumed in many of the previous related studies (Heuchel et al. 1997). For oxygen, the parameters ε/k and σ were determined as 230.0 K and 0.27 nm, respectively (Brodka and Zerda 1996). The number density of oxygen in silica is 5.982×10^{28} m^{-3} (Miyahara et al. 2000).

For the two Ar liquids, the parameters ε/k and σ were determined as 120.0 K and 0.34 nm, respectively. The mass m was 6.636×10^{-26} kg and the reduced temperature $T^* = kT/\varepsilon(\mathrm{Ar}) = 0.7$.

The thickness of the oxygen wall of Ar is 5.5σ so that Ar particles in pores do not interact with their replica by the periodic boundary condition. The position of oxygen sites were determined randomly and fixed in the region of the wall space. The pore widths W of Ar were 5.5σ, 7.5σ, and 9.5σ. The pore length was $7W$. The depth was 7σ.

The simulation run for a given number of adsorbate particles began from an initial configuration arranged as a face-

centered cubic lattice within the slit-shaped wall. The total number of particles was 3800, 5350, and 7500 for 5.5σ, 7.5σ, and 9.5σ, respectively. The total fraction of atoms in the pore space was 0.32–0.34, 0.42–0.43, and 0.47–0.48 for 5.5σ, 7.5σ, and 9.5σ, respectively. The initial velocity provided to each particle was such that the Maxwell-Boltzmann distribution was attained at the given temperature. The temperature of the system was controlled by velocity scaling in the usual manner once every 100 steps. The leapfrog Verlet method was used to integrate the equations of motion numerically. Each run comprised integration steps with a time increment of 10 fs. The total time required for each simulation was 2 μs.

The saturated concentration for the model LJ fluids was determined by a simulation of the liquid state, as described below; using the concentration, the equilibrium concentration was normalized to yield the relative concentration.

The equilibrium bulk concentration was determined by the running average (1 μs–2 μs, once for every 10 steps) of particle numbers in the region of $7\sigma < |y| < 14\sigma$ from the edge of the pore wall. Similarly, the concentration of the pore fluid was determined by the running average (1 μs–2 μs) of particle numbers in the region of $0 < |x| < 0.5\sigma$ and $0 < |y| < 10\sigma$.

3 Results and discussion

Several simulations were conducted for each pore size with various numbers of particles to obtain the liquid phase adsorption equilibrium relation. Figure 2 shows snapshots of molecules for a pore with a width of 7.5σ: (a) $N_A = 4500$, $N_B = 850$, $C/C_s = 0.238$, (b) $N_A = 3850$, $N_B = 1500$, $C/C_s = 0.703$, (c) $N_A = 3500$, $N_B = 1850$, $C/C_s = 0.708$, (d) $N_A = 2850$, $N_B = 2500$, $C/C_s = 0.860$. The black particles denote pore atoms (oxygen); the red particles, weak interactive Ar(A) with a pore wall; and the blue particles, strong interactive Ar(B). The surface adsorption phase is observed for low relative concentrations, and the separation phase develops under high relative concentrations. The important point to be noted here is that the surface adsorption state (b) and the separated state (c) show almost the same equilibrium bulk concentration despite the complete difference in the adsorbed state. This equality implies that the isotherm is almost vertical at this bulk concentration.

The averaged densities of the fluid in the pores in the central portion of the cell, where the density is not affected by the interface, were evaluated from the data obtained after 1 μs and plotted against the relative concentrations in Fig. 3. An almost vertical change in the density can be recognized for each pore size. The critical separation concentration was determined from the increase in the isotherms.

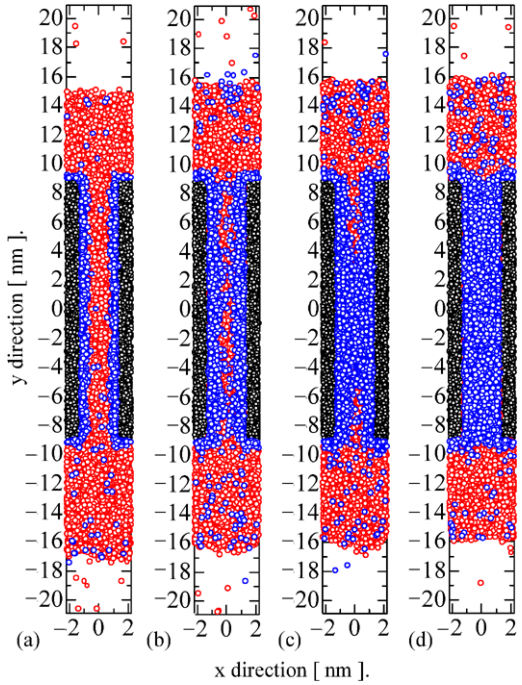

Fig. 2 Snapshots obtained by the MD simulations for a pore with a width of 7.5σ

4 Physical properties of the model fluid

To test the present model, some physical properties of the model adsorbate employed in the simulations must be known. These properties include the saturated concentration in the bulk, volume per molecule, liquid–liquid interfacial tension, and distance between the equimolar dividing surface and the surface of tension (Tolman's length or dividing thickness) within the interfacial region. The cut-off distances of the bulk LJ-Ar liquids are constant at 3.5σ.

In general, particularly for a gas-liquid surface, the interfacial tension is considered to be a function of the curvature because the radius of curvature of the curved interface in nanopores is comparable with the thickness of the gas-liquid boundary layer; the curved interface gives rise to a considerable difference in the surface tension as compared to the surface tension for a flat interface. The relation given by the Gibbs-Tolman-Koenig-Buff equation (Tolman 1948, 1949a, 1949b; Kirkwood and Buff 1949; Buff and Kirkwood 1950) is adopted for the dependence.

To make the interface inevitably, we employed the NVT-MD method. We simulated a liquid film consisting of two layers of fluids in a rectangular cell. We set up a system comprising 3000 Ar(A) particles and 6000 Ar(B) particles in a box with dimensions $L_x \times L_y \times L_z = 14.0\sigma \times 117.6\sigma \times 15.2\sigma$ on the basis of the literature (Nijmeijer et al. 1988; Holcomb et al. 1993; Chen 1995; Trokhymchuk and Alejandre 1999). Similar to the simulations performed for a pore, a border plane with an imaginary gas phase was placed in a

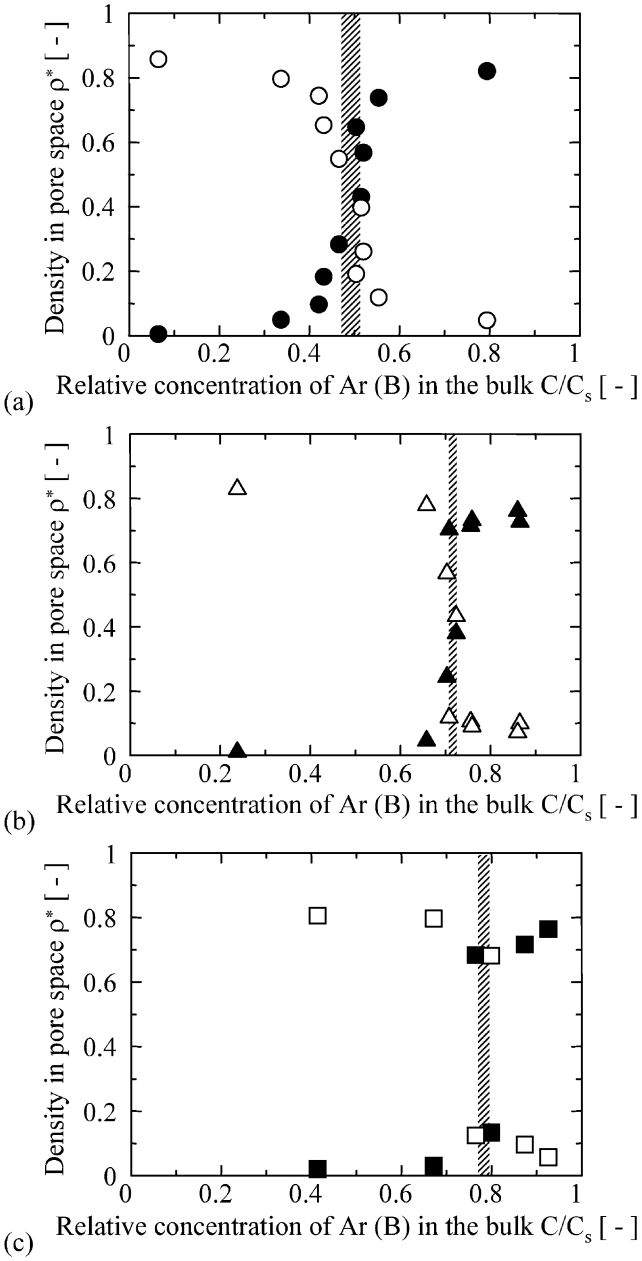

Fig. 3 Adsorption isotherms obtained using MD simulations. The CPSs are indicated by the vertical striped lines; (**a**) $W = 5.5\sigma$, (**b**) $W = 7.5\sigma$, and (**c**) $W = 9.5\sigma$

vertical direction at each end of the cell and at a sufficient distance from the liquid film. The run comprised integration steps of 10 fs.

For capillary condensation, the surface tension is treated as a function of the curvature because the radius of the curved interface in nanopores is comparable with the thickness of the liquid-liquid boundary layer; the curved interface gives rise to a considerable difference in the interfacial tension as compared to that for a flat interface. The relation provided by the Gibbs-Tolman-Koenig-Buff equation is adopted for the dependence (Yoshioka et al. 1997; Miyahara et al. 1997a, 1997b, 2000; Kanda et al. 2000a, 2000b). Therefore, this relation should also be considered in CPS.

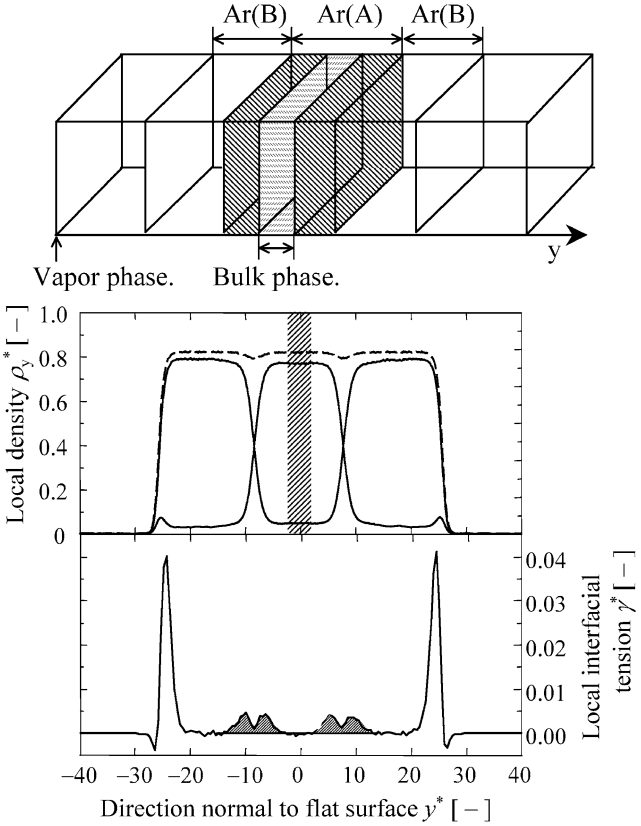

Fig. 4 Unit cell, local density and local interfacial tension of the two Ar liquids

The local interfacial tension was calculated for sliced spaces of $L_x \times 0.1\sigma$ (Ar) $\times L_z$ with the following statistical mechanical expression:

$$\gamma = \frac{1}{L_x L_z} \left\langle \sum_{i \neq j} \frac{r_{ij}^2 - 3y_{ij}^2}{r_{ij}} \frac{\mathrm{d}u(r_{ij})}{\mathrm{d}r_{ij}} \right\rangle \tag{2}$$

The interfacial tension γ was obtained by the summation of the local interfacial tension over the interfacial region (Nijmeijer et al. 1988).

Each property was determined by the running average from 1 μs to 2 μs once every 10 steps. Each property was almost constant after 1 μs.

The local density and local surface tension are shown in Fig. 4. The equimolar dividing surface was determined by using the local density profile. Two symmetric solid lines show the densities of Ar(A) and Ar(B). The broken line shows the total density. Further, the reduced saturated concentration C_s for the total density in the bulk was 0.0457 in the region $0\sigma < |y| < 2.5\sigma$.

In the interface region, we observe four surfaces of tension on both sides of the two equimolar dividing surfaces.

On a macro scale, the sum of the two tensions should be recognized as the interfacial tension. Therefore, from the summation of the four small peaks, the reduced interfacial tension γ^* was determined to be 0.211. Further, the Tolman's length δ^* was 3.75.

In the curved interface region, the surface tension, which is located more toward the interior as compared to the inner surface of tension, depends on the curvature according to the following equation:

$$\frac{\gamma_c(\rho)}{\gamma} = \frac{1}{2} \times \left(1 + \frac{\delta}{\rho_A}\right) \tag{3}$$

Here, γ_c denotes the interfacial tension at the surface of tension. ρ_A denotes the local radius of the surface of tension, as shown in Fig. 5. The values of δ and ρ_A are considered to be positive. Similarly, for the outer surface of tension,

$$\frac{\gamma_c(\rho)}{\gamma} = \frac{1}{2} \times \left(1 + \frac{\delta}{-\rho_B}\right) \tag{4}$$

since Ar(B) plays a major role in the inner surface-of-tension while Ar(A) plays a major role in the outer surface-of-tension. ρ_A is positive for the inner surface of tension (3), while ρ_B is negative for the outer surface of tension (4). The sum of these equations is as follows:

$$\frac{\gamma_c(\rho)}{\gamma} = \frac{1}{2} \times \left\{\left(1 + \frac{\delta}{\rho_A}\right) + \left(1 + \frac{\delta}{-\rho_B}\right)\right\} \tag{5}$$

However, as compared to the thickness of the surface adsorbed film of Ar(B), δ^* was considerably greater, as shown in Fig. 5. The surface of tension of Ar(B) sank into the pore wall. Similarly, for a small pore, the surface of tension of Ar(A) may intersect the surface of tension of the opposite side. Due to these problems, (5) cannot be resolved.

In this system, the potential of pore walls affect the CPS phenomenon materially. The interfacial tension has a very small effect.

Therefore, we assumed that $\rho_A = \rho_B$ with the local radius of the equimolar dividing surface. This equation implies that the Gibbs-Tolman-Koenig-Buff equation is not applicable to the CPS phenomenon.

5 Modified capillary phase separation model

We propose a new CPS model in which the force field external to the pore is considered. In order to retain simplicity, the fluid in a pore is treated as a continuum throughout.

By including the abovementioned factor, the basic equation to describe the separation is given as follows (referring to Fig. 5):

$$kT \ln \frac{C}{C_s} = \Delta\psi(x) - v_B \frac{\gamma}{\rho(x)} \tag{6}$$

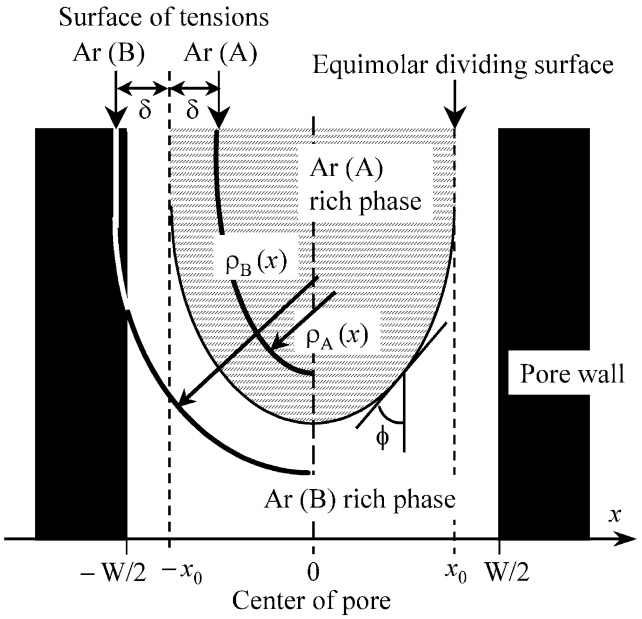

Fig. 5 Schematic figure of liquid–liquid interface in a nanopore considered for the model

Here γ denotes the interfacial tension. For γ, we assume that the bulk value is applicable to the condensate since it is very difficult to calculate the interfacial tension of heterogeneous condensates. $\rho(x)$, the local radius at a vertical position against the pore wall x; and $\Delta\psi(x)$, the contribution of the attractive potential energy of the pore wall, which must be expressed as an "excess" amount when compared with the potential energy between the strong interactive Ar liquids. The details of the influence of the cut-off distance against $\Delta\psi(x)$ is specified in previous studies (Miyahara et al. 2000; Kanda et al. 2000a).

In principle, (6) determines the local curvature term for a given relative concentration. Thus, geometrical integration with respect to the shape of the interface can be performed, which will give the size of the pore if summed with the thickness of the adsorbed film on the interior surface of the pore. Thus, the relation between the critical pore size and the equilibrium bulk concentration can be obtained. This procedure is quantitatively expressed below.

By considering the origin of ρ to be at the center of a pore, as in Fig. 5, the curvature of the interface is expressed as follows:

$$\rho(x) = \frac{dx}{d\cos\theta} \tag{7}$$

By rearranging (6) to obtain $\rho(x)$ and substituting (7), we have

$$\frac{d\cos\theta}{dx} = \frac{1}{\gamma} \times \frac{1}{v_B}\left\{\Delta\psi(x) - kT \ln\left(\frac{C}{C_s}\right)\right\} \tag{8}$$

This equation will give the shape of the meniscus. The boundary conditions for forming the interface with a con-

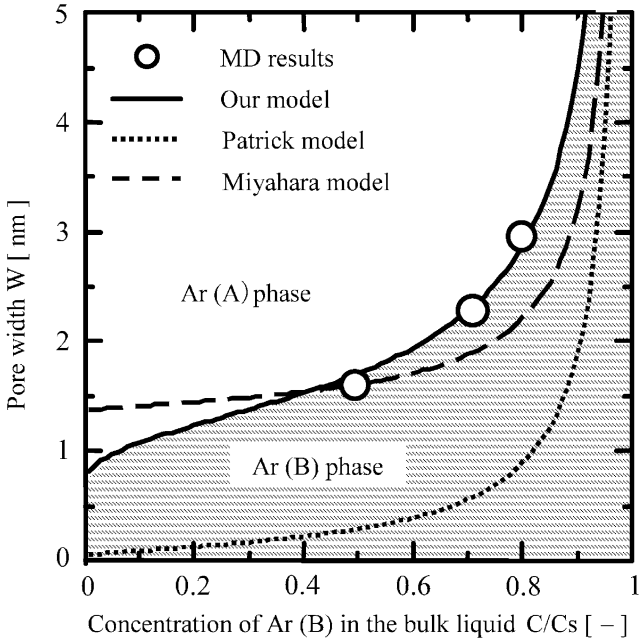

Fig. 6 Liquid-liquid coexistence curves of the two Ar liquids in slit oxygen nanopores

tact angle of zero are given by:

B.C. 1: at $x = x_0,\ \theta = 0$

B.C. 2: at $x = 0,\ \theta = \pi/2$

By formally integrating (8), and applying the above boundary conditions, we obtain the constraint to be satisfied at the critical separation condition as follows:

$$1 = \int_0^{x_0} \mathrm{d}x \frac{1}{\gamma} \times \frac{1}{v_\mathrm{B}} \left\{ \Delta\psi(x) - kT \ln\left(\frac{C}{C_\mathrm{s}}\right) \right\} \tag{9}$$

The position of the surface adsorbed film on the wall, x_0, is assumed to be given by the following equation since $1/\rho$ is 0.

$$kT \ln \frac{C}{C_\mathrm{s}} = \Delta\psi(x_0) \tag{10}$$

In summary, (9) and (10) should be solved simultaneously and numerically to determine W, t $(= W - x_0)$, and $\rho(x)$ for a given relative concentration.

The performance of the present model in predicting the critical separation concentration for a given pore size is tested here using the above results of MD simulations.

By using the bulk physical properties, the critical separation concentration for each pore size is calculated by using the present model and compared with the simulation results together with the Patrick and the Miyahara models. As shown in Fig. 6, the proposed model (solid line) predicts almost perfectly the results of the MD simulations (open circles), which shows its reliability. On the other hand, a significant underestimation of the pore size is recognized for the Patrick model (dashed line). Further, the Miyahara model cannot estimate all the MD results.

6 Conclusion

We proposed a modified CPS model for slit-shaped nanopores that considers the effect of the attractive potential energy of the pore walls. For the verification of the separation model, MD simulations were conducted to determine the critical separation concentration for various sizes of pores. By using simple concepts and handy calculations, the model successfully described the liquid-liquid coexistence relation provided by the MD simulations for nanopores.

For strong interfacial tension, the integration of Gibbs-Tolman-Koenig-Buff effect is an important issue in the future.

References

Brochard, F., De Gennes, P.G.: J. Phys. Lett. **44**, L785–L791 (1983)
Brodka, A., Zerda, T.W.: J. Chem. Phys. **104**, 6319–6326 (1996)
Buff, F.P., Kirkwood, J.G.: J. Chem. Phys. **18**, 991–992 (1950)
Chen, L.: J. Chem. Phys. **103**, 10214–10216 (1995)
De Gennes, P.G.: J. Phys. Chem. **88**, 6469–6492 (1984)
Gelb, D., Gubbins, K.E.: Phys. Rev. E **56**, 3185–3196 (1997a)
Gelb, D., Gubbins, K.E.: Phys. Rev. E **55**, R1290 (1997b)
Gelb, D., Gubbins, K.E.: Physica A **244**, 112–123 (1997c)
Goada, W.T., Gubbins, K.E., Panagiotopoulos, A.Z.: Mol. Phys. **84**, 825–834 (1995)
Heuchel, M., Snurr, R.Q., Buss, E.: Langmuir **13**, 6795–6804 (1997)
Holcomb, C.D., Clancy, P., Zollweg, J.A.: Mol. Phys. **78**, 437–459 (1993)
Kanda, H., Miyahara, M., Higashitani, K.: Langmuir **16**, 6064–6066 (2000a)
Kanda, H., Miyahara, M., Yoshioka, T., Okazaki, M.: Langmuir **16**, 6622–6627 (2000b)
Keblinski, P., Ma, W.-L., Maritan, A., Kopik, J., Banavar, J.R.: Phys. Rev. E **47**, R2265–R2268 (1993)
Kirkwood, J.G., Buff, F.P.: J. Chem. Phys. **17**, 338–343 (1949)
Laradji, M., Toxvaerd, S., Mouritsen, O.G.: Phys. Rev. Lett. **77**, 2253–2256 (1996)
Lin, A.J., Durian, D.J., Herbolzheimer, E., Safran, S.A.: Phys. Rev. Lett. **65**, 1897–1900 (1990)
Ma, W.-J., Maritan, A., Banavar, J.R., Kopik, J.: Phys. Rev. A **54**, R5347–R5350 (1992)
Miyahara, M., Kato, M., Okazaki, M.: AIChE J. **40**, 1549–1557 (1994)
Miyahara, M., Suzuki, K., Okazaki, M.: J. Chem. Eng. Jpn. **30**, 683–690 (1997a)
Miyahara, M., Yoshioka, T., Okazaki, M.: J. Chem. Phys. **106**, 8124–8134 (1997b)
Miyahara, M., Kanda, H., Yoshioka, T., Okazaki, M.: Langmuir **16**, 4293–4299 (2000)
Nakanishi, H., Fisher, M.E.: J. Chem. Phys. **78**, 3279–3292 (1983)
Nijmeijer, M.J.P., Bakker, A.F., Bruin, C., Sikkenk, J.H.: J. Chem. Phys. **89**, 3789–3792 (1988)

Patrick, W.A., Eberman, N.F.: J. Phys. Chem. **29**, 220–228 (1925)
Patrick, W.A., Jones, D.C.: J. Phys. Chem. **29**, 1–10 (1925)
Sliwinska-Bartkowiak, M., Sowers, S.L., Gubbins, K.E.: Langmuir **13**, 1182–1188 (1997)
Strickland, B., Leptoukh, G., Roland, C.: J. Phys. A: Math. Gen. **28**, L403–L408 (1995)
Tolman, R.C.: J. Chem. Phys. **16**, 758–774 (1948)
Tolman, R.C.: J. Chem. Phys. **17**, 118–127 (1949a)
Tolman, R.C.: J. Chem. Phys. **17**, 333–337 (1949b)
Trokhymchuk, A., Alejandre, J.: J. Chem. Phys. **111**, 8510–8523 (1999)
Valiullin, R., Furo, I.: Phys. Rev. E **66**, 031508 (2002)
Velasco, E., Toxvaerd, S.: Phys. Rev. E **54**, R605–610 (1996)
Yoshioka, T., Miyahara, M., Okazaki, M.: J. Chem. Eng. Jpn. **30**, 274–284 (1997)
Zhang, A., Chakrabarti, A.: Phys. Rev. E **50**, R4290–R4293 (1994)
Zhang, A., Chakrabarti, A.: Phys. Rev. B **52**, 2736–2741 (1995)